# Structure and Orientation of the Oxygen-Evolving Manganese Complex of Green Algae and Higher Plants Investigated by X-ray Absorption Linear Dichroism Spectroscopy on Oriented Photosystem II Membrane Particles†

H. Schiller,‡,§ J. Dittmer,‡ L. Iuzzolino,‡,§ W. Dörner,‡,§ W. Meyer-Klaucke,‖ V. A. Solé,⊥,▽ H.-F. Nolting,⊥ and H. Dau*,‡

*FB Biologie/Botanik and FB Chemie, Philipps-Universität Marburg, Lahnberge, D-35032 Marburg, Germany, European Molecular Biology Laboratory, Hamburg Outstation, Notkestrasse 85, D-22603 Hamburg, Germany, and HASYLAB, Notkestrasse 85, D-22603 Hamburg, Germany*

*Received September 18, 1997; Revised Manuscript Received February 10, 1998*

ABSTRACT: X-ray absorption spectroscopy at the Mn K-edge has been performed on multilayers of photosystem II-enriched fragments of the native thylakoid membrane prepared from a higher plant (spinach) and a unicellular green alga (*Scenedesmus obliquus*). Spectra collected for various angles between the prevailing orientation of the thylakoid membrane normal and the X-ray electric field vector contain information on the atomic structure of the tetranuclear manganese complex of photosystem II (PS II) and its orientation with respect to the membrane normal. The previously used approach for evaluation of the dichroism of extended X-ray absorption fine structure (EXAFS) spectra [George, G. N., et al. (1989) *Science 243*, 789−791] is modified, and the following results are obtained for PS II in its dark-stable state ($S_1$-state): (1) structure and orientation of the PS II manganese complexes of green algae and higher plants are highly similiar or fully identical; (2) two 2.7-Å vectors, which, most likely, connect the Mn nuclei of a planar $Mn_2(\mu\text{-}O_2)$ structure, are at an average angle of 80° ± 10° with respect to the thylakoid normal; (3) the plane of the $Mn_2(\mu\text{-}O_2)$ structures is rather in parallel with the thylakoid plane than perpendicular. Structural models for the oxygen-evolving manganese complex and its orientation in the thylakoid membrane are discussed within the context of the presented results.

Photosystem II (PS II), a pigment−protein complex of more than 250 kDa molecular mass, utilizes the energy of four successively absorbed photons to drive the oxidation of water (2 $H_2O$), the concomitant release of molecular oxygen (1 $O_2$), and the reduction of plastoquinone (2 PQ) to plastohydroquinone (2 $PQH_2$) (*1*−*6*). Photosynthetic water oxidation and dioxygen release take place in a section (or a functional unit) of the PS II usually called the "oxygen-evolving complex" (OEC). The OEC is assumed to contain the so-called manganese complex which consists of four manganese atoms ligated by amino acid residues of the D1−D2 heterodimer of PS II and pairwise interconnected by bridging oxygens (*2*, *7*, *8*). Detailed investigations on the kinetics of OEC charge accumulation and oxygen and proton release are suggestive of an intricate process (see, e.g., refs *4* and *9*), but in the absence of sufficient structural information mechanistic models (*3*, *9*−*14*) are likely to remain speculative.

Detailed structural information on the PS II manganese complex is obtainable by X-ray absorption spectroscopy (XAS) at the manganese K-edge. Mainly on the basis of XAS results, Klein, Sauer, Yachandra, and their co-workers (*8*, *15*) proposed a structural model of the PS II manganese complex in its $S_1$- and $S_2$-state: two di-$\mu$-oxo-bridged binuclear Mn units are connected by one mono-$\mu$-oxo bridge and two bis-carboxylato bridges such that a cis−cis arrangement of the four manganese atoms is obtained. This "Berkeley model" has gained considerable attention. It has already entered chemistry textbooks (*16*), and it has been the basis for models on the mechanism of photosynthetic water oxidation (*3*, *12*, *14*). Nonetheless, presently the arrangement of the two di-$\mu$-oxo-bridged $Mn_2$ blocks is still hypothetical (as pointed out in ref *17*).

Conventional EXAFS spectroscopy on suspensions of metalloproteins provides the distances between the absorbing metal atom and the backscattering atoms of the first, second, and, occasionally, third coordination sphere with high

† This research was supported by the German Bundesministerium für Bildung und Forschung (program: Erforschung kondensierter Materie, Verbund 48) and the Deutsche Forschungs-Gemeinschaft (Marburger Graduiertenkolleg "Enzymchemie"). H.S. and W.D. received financial support in the form of a fellowship of the Studienstiftung des deutschen Volkes.

* To whom correspondence should be addressed. Phone: +49-6421-282078. Fax: +49−6421−282057. E-mail: dauh@mailer.uni-marburg.de.

‡ FB Biologie/Botanik, Philipps-Universität Marburg.

§ FB Chemie, Philipps-Universität Marburg.

‖ HASYLAB.

⊥ European Molecular Biology Laboratory.

▽ Present address: ESRF, BP. 220, 38043 Grenoble Cedex, France.

[1] Abbreviations: Chl, chlorophyll; $Cyt_{b559}$, cytrochrome which is an integral part of PS II; EPR, electron paramagnetic resonance; EXAFS, extended X-ray absorption fine structure; HEPES, 4-(2-hydroxyethyl)-1-piperazineethanesulfonic acid; MES, 4-morpholineethanesulfonic acid; OEC, oxygen-evolving complex; PS, photosystem; $Tyr_D$, specific tyrosine residue of the PS II; XAS, X-ray absorption spectroscopy.

S0006-2960(97)02329-5 CCC: $15.00 
Published on Web 05/02/1998

precision (about 0.02 Å). However, absorber−backscatterer distances do not uniquely define the topology of a metal complex and its orientation with respect to the protein; angle information is lacking. A promising approach to obtain some orientational information is EXAFS spectroscopy on preparations of protein particles with a preferential orientation for at least one protein-intrinsic coordinate axis (*18*−*22*). By collecting EXAFS data sets for several angles between the electric field vector (of the exciting X-ray beam) and the normal of the partially oriented sample (linear dichroism spectroscopy), the angle between the absorber−backscatterer vector and the oriented protein axis becomes an experimentally accessible quantity.

The dichroism approach enhances the potential of XAS for structural investigations on uncrystallized metalloproteins. However, sample preparation and data evaluation require, in comparison to solution EXAFS, extra efforts and considerations. In previous XAS linear dichroism investigations on the PS II manganese complex (*18*, *20*, *21*), the obtained orientation information had been affected by subtle errors in the theoretical approaches used to determine (1) the extent of orientation, the mosaic spread characteristics, and (2) the orientation of the absorber−backscatterer vector (see Discussion). Here, progress is achieved by using corrected theoretical approaches. Furthermore, improvements with respect to the preparation of oriented XAS samples permit, for the first time, evaluation of the dichroism of the 1.8-Å Mn-$\mu$-O EXAFS interaction.

Various evolutionarily diverse organisms are capable of photosynthetic water oxidation: cyanobacteria, eukaryotic algae, lower and higher plants. McDermott et al. (*23*) and DeRose et al. (*17*) compared the PS II manganese complexes of spinach and the thermophilic cyanobacterium *Synechococcus* using X-ray absorption spectroscopy. They have not found indications for significant structural differences. On the other hand, EPR spectra of donor side redox factors point toward structural differences (*24*−*27*). In particular, subtle, but reproducible, differences in the so-called $S_2$-state multiline signal between PS II preparations of higher plants (spinach, barley) and unicellular green algae (*Scenedesmus obliquus*, *Chlamydomonas reinhardtii*) hint toward structural differences in the PS II manganese complex or its protein environment (*26*; unpublished results). It is one objective of the present investigation to compare structure and orientation of the PS II manganese complex of the unicellular green alga *S. obliquus* and the higher plant *Spinacia oleracea* (spinach).

For unicellular green algae, in particular *C. reinhardtii*, protocols for efficient site-directed mutagenesis of PS II proteins exist (*28*, *29*); mutagenesis studies on structure and function of the PS II donor side of green algae can be anticipated. Higher plants are not equally well-suited for site-directed mutagenesis studies, which is unfortunate because the vast majority of available experimental results on photosynthetic water oxidation have been obtained for the higher plant PS II. In this context it is of obvious importance to answer the question whether higher plants and green algae differ in the structure of the PS II manganese complex or its protein environment.

In summary, the present investigation serves two purposes: first, to compare the structures of the PS II manganese complexes of unicellular green algae and higher plants; and, second, to present detailed structural information on the PS II manganese complex in its $S_1$-state using a corrected EXAFS dichroism approach.

## MATERIALS AND METHODS

*Sample Preparation.* For preparation of PS II-enriched membrane particles, the protocol described elsewhere (*21*) has been modified as outlined in the following. Triton X-100 incubation was done in buffer A (1 M glycine betaine, 15 mM NaCl, 10 mM $MgCl_2$, and 25 mM HEPES, pH 6.0) with a detergent-to-chlorophyll ratio of 25 mg/mg of Chl. The incubation suspension was stirred gently for 20 min in an ice bath in the dark and was then spun for 3 min at 1000*g* and for 17 min at 48000*g*. After 3−5 washing steps (resuspension in buffer A and centrifugation), the PS II particles were resuspended in buffer B (400 mM sucrose, 30 mM NaCl, 5 mM $MgCl_2$, 5 mM $CaCl_2$, and 50 mM MES, pH 6.0) and spun for 30 min at 48000*g*. The Chl concentration of these pellets was 40−50 mg/mL, and the $O_2$ evolution rates were 900−1300 $\mu$mol of $O_2$/(mg of Chl)(h). The rate of oxygen evolution was assayed polarographically at 28 °C in 1 M glycine betaine, 50 mM NaCl, 2 mM $MgCl_2$, 20 mM MES (pH 6.0), 5 mM $K_3[Fe(CN)_6]$, and 0.3 mM DCBQ.

The preparation of *S. obliquus* PS II particles requires additional modifications. Thylakoids were isolated after breaking the cells in a cell mill (*30*). The Triton incubation time was 15 min using a detergent-to-chlorophyll ratio of 12.5 mg/mg of Chl. PS II particles were additionally purified by centrifugation in a Percoll gradient (25− 45%, 20 min at 30000*g*). The pellets had a concentration of about 25−30 mg of Chl/mL, and the activity of the particles measured at 28 °C was 800−1100 $\mu$mol of $O_2$/(mg of Chl)(h).

To produce samples with a preferential orientation of the membrane normal, the PS II particle pellet was transferred into acrylic glass frames (inner dimensions: 15 × 2.5 × 1 or 2 $mm^3$) with a back wall of thin Kapton tape. Using special inserts for the centrifuge rotor (made by the mechanics workshop of the FB Biologie, Marburg), the filled frames were spun in a swing-out rotor for 2 h at 130000*g* and 2 °C. Then they were dried for 12 h at 4 °C in the dark at an estimated 90% humidity. Samples were stored in liquid nitrogen.

*Sample Characterization by EPR.* The extent of orientation of the membrane particles was judged by inspection of the angle dependence of the cytochrome $b_{559}$ ($Cyt_{b559}$) and the $Tyr_D^+$ EPR signals (*31*). It was also verified for each sample that there was no contamination by adventitious $Mn^{II}$. By using control samples from the same batch of oriented samples used later for XAS measurement, we verified that 200 K illumination causes formation of the multiline signal (*32*).

*Collection of X-ray Absorption Data*. EXAFS and edge spectra were collected at the EMBL beam line D2, a bending magnet beam line, at HASYLAB (DESY, Hamburg, Germany) using a focused beam and a Si(111) monochromator (beam size on the sample: 3−6 mm width and 1 mm height). Moving the sample in the vertical direction allowed irradiation of two distinct regions of the sample. An absolute energy calibration was performed by monitoring the Bragg reflections of a crystal positioned at the back end of the beam line (*33*). During the XAS measurements the samples were

kept at 17−20 K using a closed-cycle helium cryostat. Rotation of the sample holder allowed the precise adjustment (estimated error, ±1.5°) of the angle, $\Theta_E$, between the sample normal and the X-ray electric field vector.

X-ray fluorescence excitation spectra were collected using a 13-element solid-state detector (Canberra Instruments, Meriden) operated in an energy-resolving single-photon-counting mode. The total count rate per element channel was 1000−5000 counts/s. After amplification, the signal of each channel passed a single-channel analyzer with the energy window set to capture about 90% of the manganese Kα fluorescence. For spinach samples we obtained count rates (summation over all 13 channels) of 12 000 and 2000 counts/s at the excitation angles 15° and 75°, respectively. For the green alga, the count rates were significantly lower (by about a factor of 2).

In the case of dilute samples, X-ray fluorescence spectra are closely related to the corresponding absorption spectra. For the sake of simplicity, in the following all spectra are referred to as X-ray absorption spectra. Spectra were collected for various angles, $\Theta_E$, between the X-ray electric field vector and the normal of the Kapton foil which carried the PS II membrane particles. Data points were collected in steps of 0.7−0.9 eV for EXAFS spectra (in the EXAFS region) and every 0.15 eV for edge spectra (in the edge region). The collection time varied between 1 and 1.5 s per point. The results of several energy scans were averaged (see below); a single scan lasted 30−45 min. For $\Theta_E$ = 15° or 35° typically 15 scans were averaged; for $\Theta_E$ = 55° or 75° typically 40 scans were averaged.

Two data collection approaches were used which differ with respect to the beam exposure time for the individual samples.

(I) The first approach involved collection of all scans for a given excitation angle on the same sample. For $\Theta_E$ = 55° or 75° two positions of the beam on the same sample were used. Consequently, a single spot of the sample surface had been exposed to the X-ray beam for 10−15 h.

(II) The second approach involved frequent sample changes such that the maximal X-ray exposure time was below 2.5 h for $\Theta_E$ = 55° or 75° and below 3.5 h for $\Theta_E$ = 15° or 35°.

*Data Processing and Evaluation*. After correction of the energy scale, equivalent scans were averaged. The slope of the pre-edge scattering background was close to zero. Therefore, subtraction of a constant value was sufficient to remove the pre-edge background. In the post-edge range the hypothetical EXAFS-free absorption, $\mu_0$, was determined by a second-order polynomial fit. For normalization the spectra were divided by this polynomial. For extraction of EXAFS spectra, the background was removed by subtraction of a cubic spline (3 segments, knots separated by 178 eV). The energy axis (*E*-space) of the EXAFS spectra was converted to an equidistant wavenumber axis (*k*-space) according to

$$k = \sqrt{\frac{2m_e(E - E_0)}{\hbar^2}}$$

with $E_0$ = 6540 eV. The transition to an equidistant *k*-axis involved a reduction of the number of data points to 100. Only for Figure 3 has the number of data points been chosen to be 200. The resulting spectra ($\chi(k)$ versus *k*) were weighted by $k^3$. All *R*-space spectra shown in the figures were obtained by Fourier transformation of $k^3$-weighted data corresponding to the energy range 6555−7100 eV. For these transformations a fractional cosine window was used (at the low-*k* side and at the high-*k* side the window extends over 10% of the *k* range).

For the so-called Fourier isolation (or Fourier filtering), $k^3$ data corresponding to the energy range 6560−7080 eV was utilized for the *k*-to-*R* Fourier transformation. (We found that by the use of a relatively large *k* range for the *k*-to-*R* Fourier transform, artifacts are minimized when the Fourier isolation approach is used.) For the *R*-to-*k* transformation a rectangular window function was employed; the window borders were chosen to match the usually well-resolved minimum between two peaks of the *R*-space spectrum. For curve fitting of the Fourier-isolated EXAFS oscillations, *k*-space data was used which corresponds to the energy range 6582−7010 eV.

Curve fitting and Fourier filtering of EXAFS spectra was performed using the program EXCURV92 (BIOSYM/MSI, San Diego, CA). EXAFS calculations were carried out using the curved-wave theory of Gurman et al. (*34*). Potentials for the EXAFS phase functions were calculated with the Xalpha method for ground state and exchange potentials (common interstitial potential of −20 eV; central atom in the relaxed state; imaginary potential of −4 eV; amplitude reduction factor of 0.8). By a least-squares fit of the calculated EXAFS, $\chi^{exp}(k_i)$, to the data points, $\chi^{th}(k_i)$, the coordination number, *N*, the distance, *r*, and the Debye−Waller parameter, $2\sigma^2$, were determined for each backscatterer shell. The *R*-factor given in Tables 1−5 is defined as

$$R = \frac{\sum_{i=1}^{n} k_i^{\nu} |\chi^{exp}(k_i) - \chi^{th}(k_i)|}{\sum_{j=1}^{n} k_j^{\nu} |\chi^{exp}(k_j)|} \times 100\% \qquad (1)$$

with the weighting exponent, $\nu$, and both summations over *n* data points.

## RESULTS

*Assessment of Mosaic Spread*. For quantitative assessment of the mosaic spread of the partially oriented membrane particles, EPR spectra of $Cyt_{b559}$, which is a constituent of the PS II pigment−protein complex, were collected for at least 10 angles between the magnetic field vector and the sample normal (at 20 K, microwave power of 1 mW). Then the angle dependence of the cytochrome $g_y$ and $g_z$ signal amplitudes was simulated, assuming a Gaussian distribution function for the membrane normal, and compared to the experimental values (Figure 1). It should be noted that in previous XAS dichroism investigations (*18*, *20*, *21*) the mosaic spread had been significantly underestimated due to a methodical error in the previously used simulation approach of Blum et al. (*35*) (see Discussion).

By simulations of the detection angle dependence of the $Cyt_{b559}$ $g_z$ and $g_y$ signals, we determined the half-width of the Gaussian distribution function (the mosaic spread angle, $\Omega_{sp}$) to be 35° and 38° for preparations of spinach and *S. obliquus*, respectively.

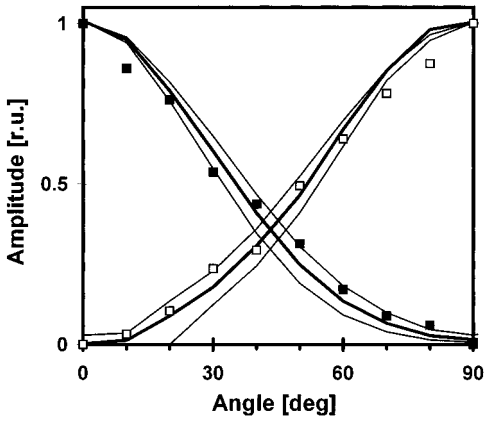


FIGURE 1: Relation between amplitudes of $Cyt_{b559}$ EPR signals and the measurement angle for partially oriented PS II membrane particles of spinach. The amplitudes of the EPR derivative spectra are shown for the $g_y$ feature (closed squares) and the $g_z$ peak (open squares) for various angles between the magnetic field vector and the sample normal. The thick line represents the simulation results for $\Omega_{sp}= 35°$; the lower and the upper thin lines show the simulation results for $\Omega_{sp}= 32°$ and $\Omega_{sp}= 38°$, respectively. The $g_y$ and the $g_z$ signal amplitudes are normalized to their values at 0° and 90°, respectively.

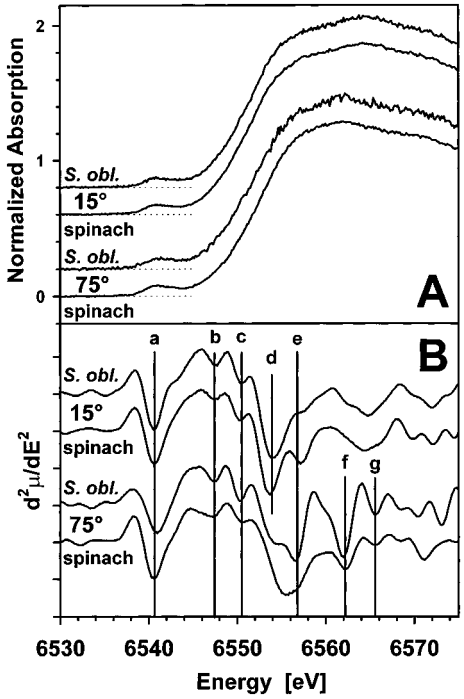


FIGURE 2: Mn K-edge spectra for oriented PS II membrane particles of spinach and the green alga *Scenedesmus obliquus* (*S. obl.*). Spectra were collected at 15° (upper two lines) and 75° (lower two lines). (A) Normalized edge spectra; (B) second-derivative spectra. The characteristic minima of the second derivative are marked by the letters *a*−*g*.

*Comparison of Edge Spectra*. Mn K-edge spectra were collected at various excitation angles for partially oriented PS II membrane particles of spinach and *S. obliquus*. Apart from the higher noise level for the *S. obliquus* spectrum at 75°, spinach and alga spectra match very well (Figure 2). In particular, the angle dependence of features d, f, and g is the same for both organisms (for a more detailed analysis of the dichroism of spinach $S_1$-state spectra, see ref *22*). Edge spectra of various synthetic manganese complexes have been studied (*3*, *8*, *15*, *36*, *37*); usually, metal complexes of different structure or oxidation state differ in their edge fine structure. Consequently, the edge fine structure can serve as a fingerprint for a particular metal center. Therefore, the observed similarity of the edge spectra is an indication that the oxidation states, the structures, and the orientations (with respect to the membrane normal) of the PS II manganese complexes of green alga and higher plants are alike.

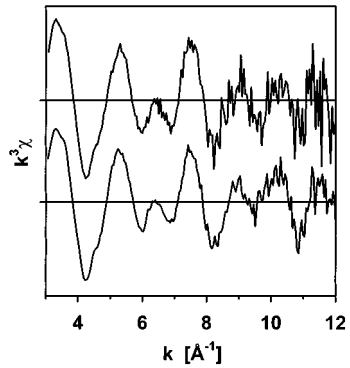


FIGURE 3: $k^3$-Weighted EXAFS spectra of the PS II manganese complexes of the green alga *S. obliquus* (upper trace) and spinach (lower trace). Both spectra were collected at 55°.

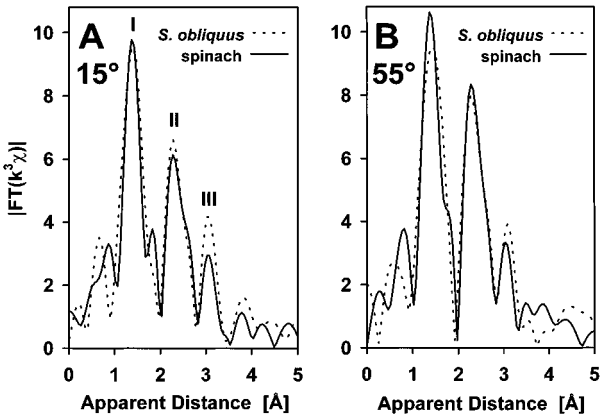


FIGURE 4: Fourier transforms of $k^3$-weighted EXAFS spectra of spinach (solid line) and *S. obliquus* (broken line) for detection at 15° (A) and 55° (B).

*Comparison of EXAFS Spectra*. Figure 3 shows $k^3$-weighted EXAFS spectra collected at 55°, which is close to the so-called magic angle of 54.7°. As predicted by eq 4 presented below, the magic angle spectra correspond closely to spectra of conventional, unoriented samples (not shown). The absence of obvious differences between the EXAFS spectra of the two organisms confirms their structural similiarity.

In Figure 4, Fourier-transformed EXAFS spectra of the green alga and the higher plant, which were collected at 15° and 55°, are compared. The Fourier-transformed EXAFS spectra exhibit three main peaks (I, II, and III in Figure 4). The two main peaks at apparent distances of 1.4 (I) and 2.3 Å (II) correspond to backscattering atoms at ∼1.8 and ∼2.7 Å, respectively. Peak I is usually assumed to originate mainly from backscattering oxygen atoms which serve as bridging ligands in a di-$\mu$-oxo-bridged, binuclear Mn structure; peak II has been assigned to the 2.7-Å Mn−Mn EXAFS interaction of the di-$\mu$-oxo-bridged Mn dimer (*3*, *8*, *36*, *38*, *39*). The origin of peak III is disputed (*17*, *40*−*42*). The Fourier peaks at distances greater than 3.5 Å provide an estimate of the noise level; the peak below 1 Å, which results

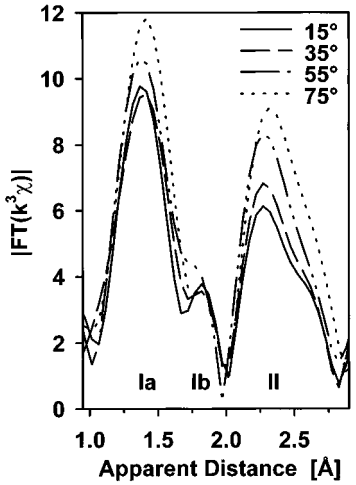


FIGURE 5: Fourier transforms of $k^3$-weighted EXAFS spectra of spinach for 4 excitation angles ($\Theta_E$ = 15°, 35°, 55°, and 75°).

from incomplete background removal, is meaningless.

Within the limits of the signal-to-noise ratio, the positions and heights of peak I and peak II of both organisms are identical at both excitation angles. This finding confirms that the orientation (with respect to the thylakoid membrane) of the PS II manganese complex of green algae and higher plants is the same. (In Figure 4, peak III is higher in the green alga. Currently we assume that this difference in the spectra of the two organisms is a noise artifact.)

*Dichroism of EXAFS Spectra.* A closer inspection of the EXAFS dichroism (Figure 5) reveals a continuous amplitude increase of peak I and peak II with increasing excitation angle. Furthermore, the shape of the Fourier peaks is changing. In particular in the case of peak I we find for an excitation angle of 15° a splitting of the first peak (peak Ia and peak Ib in Figure 5).

Fourier isolation of the first Fourier peak reveals that the corresponding EXAFS oscillations are angle dependent with respect to the shape of the oscillation envelope (Figure 6A). For the 15° data set, the EXAFS oscillation approaches a beat pattern which is indicative of backscattering atoms at two distinct distances within the first manganese coordination shell. For the second Fourier peak, it is mainly the magnitude of the EXAFS oscillations which depends on the excitation angle (Figure 6B). This finding is suggestive of pronounced variations in the (apparent) coordination number for the backscattering manganese atom at 2.7 Å.

In contrast to previous XAS linear dichroism investigations on the PS II manganese complex (*18*, *20*), we did not observe a reproducible angle dependence of the magnitude of the third Fourier peak. Therefore, quantitative evaluation of the dichroism in the 3.3-Å EXAFS interaction has not been approached.

*Curve Fitting of EXAFS Spectra.* K-space curve fitting of Fourier-isolated EXAFS spectra was done as described in Materials and Methods (see also Discussion). Multiple scattering contributions to the Fourier-isolated second peak data are not considered because such contributions are likely to be negligibly small (*43*). In Table 1 results for the Fourier-isolated second peak are shown. Table 1, section II, relates to data collected with an approach which minimizes the X-ray exposure time (approach II as described in Materials and Methods); for section I a more conventional data collection approach was used which involves X-ray exposure for up to 15 h (approach I).

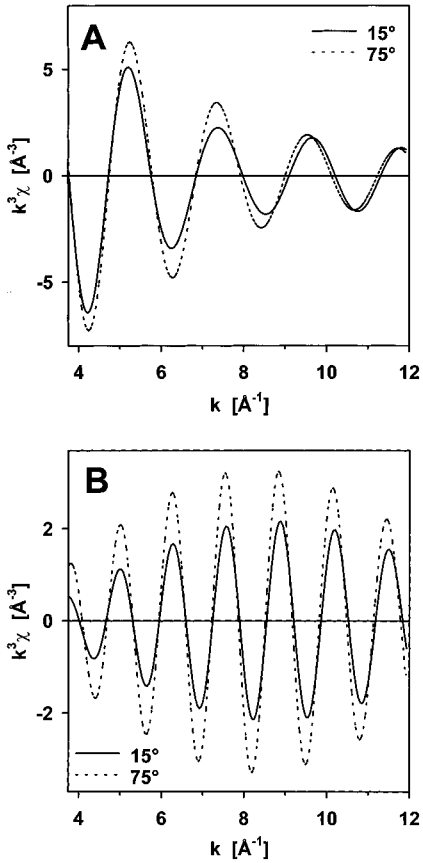


FIGURE 6: Fourier-isolated EXAFS spectra of spinach for two excitation angles, 15° (solid lines) and 75° (broken lines). EXAFS oscillations related to backscattering atoms of the first and second manganese coordination shell are shown in panels A and B, respectively. These spectra were obtained by Fourier filtering of the corresponding peaks in the *R* spectra shown in Figure 5.

Table 1: EXAFS Fit Parameters for Fourier-Isolated Peak II Data of Spinach[a]

| | Mn−Mn, 2.7 Å | | | | |
|---|---|---|---|---|---|
| $\Theta_E$ | *N* | *r* [Å] | $2\sigma^2$ [Å$^2$] | $E_0$ [eV] | *R* [%] |
| | | | I | | |
| 15° | 0.5 | 2.677 | 0.001 | 13.1 | 7 |
| 35° | 0.7 | 2.676 | 0.004 | 14.8 | 7 |
| 55° | 0.8 | 2.702 | 0.008 | 11.9 | 7 |
| 75° | 1.0 | 2.692 | 0.008 | 11.8 | 8 |
| | | | II | | |
| 15° | 0.7 | 2.688 | 0.004 | 11.6 | 6 |
| 35° | 0.8 | 2.690 | 0.005 | 11.6 | 7 |
| 55° | 1.1 | 2.691 | 0.006 | 11.3 | 8 |
| 75° | 1.3 | 2.705 | 0.007 | 10.0 | 9 |

[a] Data shown for various excitation angles, $\Theta_E$, and two distinct irradiation protocols: up to 15 h (I) and less than 2.5 h (II). Fit parameters and error, *R*, are as defined in the text.

The fit results confirm the dichroism already hinted at by the *R*-space data shown in Figures 4 and 5. The apparent coordination number (*N* in Table 1) increases with increasing excitation angle, indicating a preferential orientation of the absorber−backscatterer vector perpendicular to the membrane normal. For irradiation protocol I, due to extensive X-ray exposure "radiation damage" occurs (see also ref *22*). This radiation damage results in a decreased coordination number and an increase of the Debye−Waller parameter at

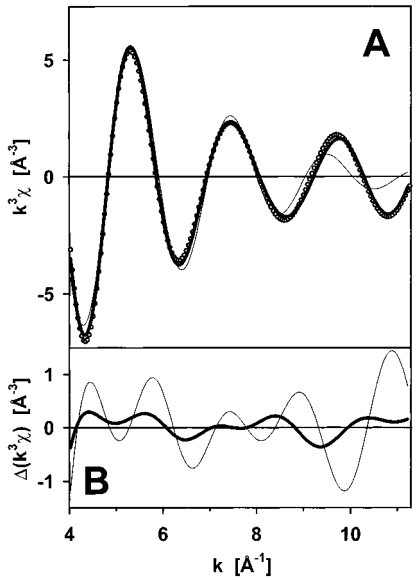


FIGURE 7: Comparison of a one-distance fit (thin lines) with a two-distance fit (thick lines) for the first coordination shell (spinach, excitation angle of 15°). In panel A the data points (open circles) and the spectra which result from the least-squares fit are shown. In panel B the difference between the experimental, Fourier-filtered spectrum and the best-fit spectrum is plotted (residual plot). The one-distance fit resulted in $N = 6.4$, $r = 1.82$ Å, $2\sigma^2 = 0.028$ Å$^2$ and $E_0 = 23.6$ eV ($R = 24\%$). The two-distance fit resulted in $N_a = 1.6$, $r_a = 1.80$ Å, $2\sigma_a{}^2 = 0.005$ Å$^2$, $N_b = 5.1$, $r_b = 1.95$ Å, $2\sigma_b{}^2 = 0.029$ Å$^2$, and $E_0 = 15.9$ eV ($R = 7\%$). In the case of the two-distance fit the distances $r_a$ and $r_b$ were fixed to match the fit results of the 55° $k^1$ spectrum fit; also, the value for the Debye−Waller factor of the distance $r_a$ had been fixed.

55° and 75°. Surprisingly, the angle dependence of the apparent coordination number is hardly affected by the prolonged X-ray exposure.

The first Fourier peak requires a two-distance fit approach. This is obvious for the 15° EXAFS oscillations. As shown in Figure 7, a one-distance fit clearly fails to match the experimental spectrum. The two-distance fit presented in Figure 7 involves fixed distances, which were obtained as described below, and a fixed Debye−Waller parameter for the shorter distance. Thus, the number of free fit parameters was not higher than for the one-distance fit ($N$, $r$, $2\sigma^2$, $E_0$), but the error sum was lower by a factor of 3.

The EXAFS oscillations corresponding to the first Fourier peak require a two-distance fit approach. However, a two-distance fit may involve up to 8 free fit parameters ($2 \times N$, $2 \times r$, $2 \times 2\sigma^2$, and 1 or $2 \times E_0$). This relatively high number of free parameters does not allow a unique solution of the minimization problem (minimization of the error sum by the fit program). Therefore, it is necessary to use physically and chemically reasonable constraints.

Considerable evidence has been presented that the PS II−Mn complex consists of two di-$\mu$-oxo-bridged binuclear Mn structures. In such a structure the Mn−$\mu$-O distance is ~1.8 Å, whereas for non-$\mu$-O ligands usually distances of 1.9−2.3 Å are found (*11*, *44*). On the basis of this consideration and assuming the absorbing Mn to be hexa-coordinated (*45*), we predict that for an isotropic sample the coordination number for oxygen ligands at 1.8 Å is 2, whereas the coordination number for ligands at larger distances (1.9−2.3 Å) is 4. Equation 4 predicts that at 54.7°, the so-called magic angle of linear dichroism spectroscopy, the angle-dependent apparent coordination number is equal to the coordination number of a (hypothetical) isotropic sample. Therefore, we decided to fit the 55° first EXAFS peak under the assumption that there is a shorter distance with a coordination number of 2 and a longer distance with a coordination number of 4. Furthermore, the Debye−Waller parameter for the shorter distance was fixed to a constant value. Using these constraints, which are reasonable but not model-independent, we obtained a unique solution of the fit problem. Subsequently, the distances obtained by this approach were used for fitting the EXAFS oscillations at all 4 excitation angles (because, to a first approximation, the distance values are independent of the excitation angle; see also Discussion). The results obtained by this curve fit approach are shown in Table 2. The angle dependence of the apparent coordination number of the 1.8-Å distance is suggestive of a preferential orientation of the corresponding absorber−backscatterer vector perpendicular to the membrane normal.

Table 2: EXAFS Fit Parameters for Fourier-Isolated Peak I Data of Spinach[a]

| | Mn−O, 1.8 Å | | Mn−O/N, 2.0 Å | | | | | |
|---|---|---|---|---|---|---|---|---|
| $\Theta_E$ | $N$ | $r$ [Å] | $2\sigma^2$ [Å$^2$] | $N$ | $r$ [Å] | $2\sigma^2$ [Å$^2$] | $E_0$ [eV] | $R$ [%] |
| | | | | I | | | | |
| 15° | 1.5 | 1.806[b] | 0.005[c] | 6.0 | 1.965[b] | 0.035 | 15.3 | 6 |
| 35° | 1.8 | 1.806[b] | 0.005[c] | 4.8 | 1.965[b] | 0.027 | 15.9 | 5 |
| 55° | 1.8 | 1.806[b] | 0.005[c] | 5.1 | 1.965[b] | 0.029 | 15.8 | 6 |
| 75° | 2.0 | 1.806[b] | 0.005[c] | 4.7 | 1.965[b] | 0.024 | 15.2 | 5 |
| | | | | II | | | | |
| 15° | 1.4 | 1.798[b] | 0.005[c] | 5.8 | 1.946[b] | 0.033 | 14.9 | 4 |
| 35° | 1.6 | 1.798[b] | 0.005[c] | 5.6 | 1.946[b] | 0.029 | 15.6 | 4 |
| 55° | 1.9 | 1.798[b] | 0.005[c] | 4.2 | 1.946[b] | 0.019 | 15.6 | 4 |
| 75° | 2.1 | 1.798[b] | 0.005[c] | 4.5 | 1.946[b] | 0.019 | 15.5 | 4 |

[a] Data shown for various excitation angles, $\Theta_E$, and two distinct irradiation protocols: up to 15 h (I) and less than 2.5 h (II). Fit parameters and error, $R$, are as defined in the text. [b] The distances obtained on the 55° data sets as described in the text were used for all other excitation angles. [c] The Debye−Waller parameter for the 1.8-Å distance was fixed to 0.005 Å$^2$.

A comparison of sections II (short X-ray exposure times) and I (exposure times of up to 15 h) of Table 2 demonstrates that prolonged X-ray exposure does not affect the dichroism of the coordination numbers. However, a considerable increase in the Debye−Waller parameter for spectra collected at 55° and 75° is observed.

The Fourier-isolation approach is debatable because Fourier transform artifacts might affect the results. To assess the significance of such artifacts, unfiltered spectra were subjected to curve fitting. With respect to the first coordination shell we used the approach described above for Fourier-isolated EXAFS oscillations. For the unfiltered data, correlations of the various fit parameters result in shallow minima of the error sum. Furthermore, the results were found to depend on the start values of the fit parameters because several local minima exist. Therefore, we consider the fit approach involving Fourier-isolated data to be superior. In any event, fit results obtained by whole-spectra fit (Table 3) are in reasonable agreement with the results obtained by fitting Fourier-isolated data. In particular, the results shown in Table 3 demonstrate clearly that the dichroism in the 1.8-Å shell does not result from a Fourier-isolation artifact.

Table 3: Parameters of EXAFS Whole-Spectra Fit for Spinach[a]

| | Mn−O, 1.8 Å | | | Mn−O/N, 2.0 Å | | | Mn−Mn, 2.7 Å | | | | |
|---|---|---|---|---|---|---|---|---|---|---|---|
| $\Theta_E$ | $N$ | $r$ [Å] | $2\sigma^2$ [Å$^2$] | $N$ | $r$ [Å] | $2\sigma^2$ [Å$^2$] | $N$ | $r$ [Å] | $2\sigma^2$ [Å$^2$] | $E_0$ [eV] | $R$ [%] |
| | | | | | II | | | | | | |
| 15° | 1.5 | 1.787[b] | 0.005[c] | 6.0 | 1.939[b] | 0.027 | 0.8 | 2.677 | 0.004 | 15.4 | 35 |
| 35° | 1.6 | 1.787[b] | 0.005[c] | 5.8 | 1.939[b] | 0.024 | 0.9 | 2.677 | 0.005 | 15.8 | 40 |
| 55° | 2.2 | 1.787[b] | 0.005[c] | 4.3 | 1.939[b] | 0.011 | 1.0 | 2.681 | 0.003 | 15.7 | 32 |
| 75° | 2.2 | 1.787[b] | 0.005[c] | 4.7 | 1.939[b] | 0.013 | 1.3 | 2.693 | 0.005 | 14.7 | 35 |

[a] Data shown for various excitation angles, $\Theta_E$, and irradiation protocol II (less than 2.5 h). Fit parameters and error, $R$, are as defined in the text. [b] The distances obtained on the 55° data sets as described in the text were used for all other excitation angles. [c] The Debye−Waller parameter for the 1.8-Å distance was fixed to 0.005 Å$^2$.

Table 4: EXAFS Fit Parameters for Fourier-Isolated Peak II Data of *Scenedesmus*[a]

| | Mn−Mn, 2.7 Å | | | | |
|---|---|---|---|---|---|
| $\Theta_E$ | $N$ | $r$ [Å] | $2\sigma^2$ [Å$^2$] | $E_0$ [eV] | $R$ [%] |
| | | | I | | |
| 15° | 0.6 | 2.666 | 0.003 | 14.8 | 6 |
| 35° | 0.7 | 2.685 | 0.004 | 14.8 | 7 |
| 55° | 0.9 | 2.714 | 0.009 | 13.1 | 10 |
| | | | II | | |
| 15° | 0.8 | 2.684 | 0.005 | 12.9 | 7 |
| 55° | 1.3 | 2.690 | 0.008 | 11.0 | 8 |

[a] Data shown for various excitation angles, $\Theta_E$, and two distinct irradiation protocols: up to 15 h (I) and less than 2.5 h (II). Fit parameters and error, $R$, are as defined in the text.

Table 5: EXAFS Fit Parameters for Fourier-Isolated Peak I Data of *Scenedesmus*[a]

| | Mn−O, 1.8 Å | | | Mn−O/N, 2.0 Å | | | | |
|---|---|---|---|---|---|---|---|---|
| $\Theta_E$ | $N$ | $r$ [Å] | $2\sigma^2$ [Å$^2$] | $N$ | $r$ [Å] | $2\sigma^2$ [Å$^2$] | $E_0$ [eV] | $R$ [%] |
| | | | | I | | | | |
| 15° | 1.8 | 1.815[b] | 0.005[c] | 4.5 | 1.979[b] | 0.029 | 15.1 | 7 |
| 35° | 2.0 | 1.815[b] | 0.005[c] | 4.9 | 1.979[b] | 0.031 | 14.7 | 6 |
| 55° | 1.9 | 1.815[b] | 0.005[c] | 4.8 | 1.979[b] | 0.027 | 14.5 | 3 |
| | | | | II | | | | |
| 15° | 1.9 | 1.770[b] | 0.005[c] | 4.1 | 1.921[b] | 0.016 | 18.7 | 8 |
| 55° | 2.1 | 1.770[b] | 0.005[c] | 3.8 | 1.921[b] | 0.011 | 18.4 | 8 |

[a] Data shown for various excitation angles, $\Theta_E$, and two distinct irradiation protocols: up to 15 h (I) and less than 2.5 h (II). Fit parameters and error, $R$, are as defined in the text. [b] The distances obtained on the 55° data sets as described in the text were used for all other excitation angles. [c] The Debye−Waller parameter for the 1.8-Å distance was fixed to 0.005 Å$^2$.

The Fourier-isolated EXAFS oscillations of the green alga *S. obliquus* were treated in a completely analogous way; the curve fit results are shown in Tables 4 and 5.

*Determination of* $\Theta_R$. In previous investigations (*18*−*21*) an inaccurate approach for $\Theta_R$ determination has been used; in the following a corrected approach is outlined.

We assume that for simulation of EXAFS data in the considered $k$-range the small-atom approximation (*46*) is sufficiently precise. This implies that for each absorber−backscatterer atom pair the magnitude of EXAFS oscillations is proportional to the squared cosine of the angle, $\Theta_{ER}$, between the X-ray electric field vector, $E$, and the vector $R$, which connects the nuclei of the absorbing and the backscattering atom (see Figure 8), whereas other characteristics of the EXAFS oscillations (in particular the apparent absorber−backscatterer distance) are independent of $\Theta_{ER}$.

The preferential orientation of the membrane normal, $M$, of the PS II membrane particles is parallel to the normal, $S$,

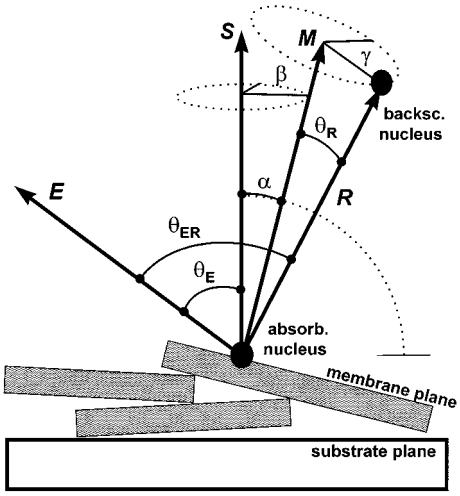


FIGURE 8: Vectors and angles relevant for X-ray absorption on metalloproteins embedded in partially oriented membrane sheets. The normals of the individual membrane sheet and the supporting substrate are denoted as $M$ and $S$, respectively. The X-ray electric field vector is labeled $E$, and the direction of the vector connecting the absorbing nucleus and the backscattering nucleus is given by $R$. To calculate the apparent coordination number for a given measurement angle ($\Theta_E$), integration over all possible orientations of the membrane normals (α- and $\beta$-integration; the dotted lines indicate the integration paths) and the cone of orientations of the absorber−backscatterer vector ($\gamma$-integration) is required.

of the supporting substrate (here a Kapton foil). It needs to be considered, however, that only imperfect vectorial orientation is obtained. For isotropic samples the probability, $P_\alpha$, to find an angle α between the membrane normal, $M$, and the substrate normal, $S$, is sin α. For imperfectly vectorially oriented samples $P_\alpha$ is assumed to be equal to the product of sin α and an order function, $P_{ord}(\alpha)$, which is maximal for an α-value of 0°. It is often assumed that $P_{ord}(\alpha)$ is well approximated by a Gaussian distribution function; its half width has been denoted as the mosaic spread angle or the disorder angle, Ω (*21*, *35*).

Now the magnitude of the EXAFS oscillations for a large ensemble of absorber−backscatterer pairs is obtainable by the $P_\alpha$-weighted integration over all orientations of the membrane normal, $M$ (α- and $\beta$-integration), and along the cone of possible orientations of $R$ with respect to $M$ ($\gamma$-integration). (Here we, reasonably, have assumed that the mosaic spread of $R$ with respect to the membrane normal is negligible, meaning that $\Theta_R$ is constant.) Thus, we obtain for the ratio between $N_{iso}$, the coordination number of an isotropic sample, and $N_{app}$, the apparent coordination number as it is found for EXAFS measurements on a partially oriented sample at an excitation angle $\Theta_E$ (see Figure 8):

$$\frac{N_{app}}{N_{iso}} = \frac{\int_0^{\pi/2}\int_0^{2\pi}\int_0^{2\pi}\cos^2\Theta_{ER}\,P_{ord}(\alpha)\sin\alpha\,d\gamma\,d\beta\,d\alpha}{\int_0^{\pi/2}\int_0^{2\pi}\int_0^{2\pi}\cos^2\Theta_{ER}\sin\alpha\,d\gamma\,d\beta\,d\alpha} \quad (2)$$

with

$$\int_0^{\pi/2} P_{ord}(\alpha)\cdot\sin\alpha\cdot d\alpha = 1 \quad (3)$$

Performing the $\beta$- and $\gamma$-integration results in

$$N_{app}(\Theta_E) = N_{iso} + {}^1/_2\,N_{iso}(3\cos^2\Theta_E - 1)\times (3\cos^2\Theta_R - 1)I_{ord} \quad (4)$$

with

$$I_{ord} = {}^1/_2\int_0^{\pi/2}(3\cos^2\alpha - 1)P_{ord}(\alpha)\sin\alpha\,d\alpha \quad (5)$$

If several absorber−backscatterer vectors are described by a common apparent coordination number, $N_{app}(\Theta_E)$, the $\Theta_R$ value of eq 4 corresponds to an average angle which is related to the orientation of the individual absorber−backscatterer angles ($\Theta\,'_R$) according to

$$\sin^2\Theta_R = \sum_{i=1}^{N_{iso}}\frac{\sin^2\Theta_R^i}{N_{iso}} \quad (6)$$

The details of the derivation of eqs 4−6 will be presented elsewhere (J. Dittmer and H. Dau, manuscript in preparation).

Assuming that $P_{ord}(\alpha)$ is well-approximated by a Gaussian distribution function, we determined half-width angles, $\Omega_{sp}$ (with $P_{ord}(\Omega_{sp}) = 0.5$), of 35° and 38° for PS II membrane particles of spinach and *S. obliquus*, respectively, by analysis of the excitation angle dependence of the $Cyt_{b559}$ EPR signal (see Figure 1 and Discussion). Using the corresponding order function, $P_{ord}(\alpha)$, we performed curve fitting of the excitation angle dependence of the apparent coordination numbers on the basis of eq 4 (see Figure 9 and Table 6).

For the various data sets shown in Table 6, the error in $\Theta_R$ which is due to the scatter in the apparent coordination numbers is estimated to be ±5°. To assess the error range which is due to the uncertainty in the mosaic spread angle (estimated uncertainty of $\Omega_{sp}$: 2°), for each data set, $\Theta_R$ values are presented for $\Omega_{sp}$ + 2°, $\Omega_{sp}$, and $\Omega_{sp}$ − 2° (Table 6).

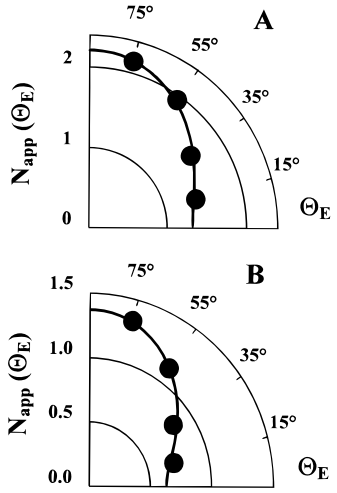


FIGURE 9: Polar plot of apparent coordination numbers versus the excitation angle, $\Theta_E$. The data points correspond to values presented in Table 1, section II (B), and Table 2, section II (A). The solid lines are calculated for $N$ and $\Theta_E$ values which have been obtained by a least-squares fit on the basis of eq 4, assuming a Gaussian order function with $\Omega_{sp} = 35°$. (A) 1.8-Å distance: $N_{iso} = 1.9$, $\Theta_{1.8\,Å} = 70°$. (B) 2.7-Å distance: $N_{iso} = 1.1$, $\Theta_{2.7\,Å} = 81°$.

Table 6: Average Angles between Membrane Normal and Distance Vectors, $\Theta_R$, and Isotropic Coordination Numbers, $N_{Iso}$, as Determined by Curve Fitting Using Equation 4[a]

| | | Mn−O, 1.8 Å | | Mn−O/N, 2.0 Å | | Mn−Mn, 2.7 Å | |
|---|---|---|---|---|---|---|---|
| | $\Omega_{sp}$ | $\Theta_R$ | $N_{iso}$ | $\Theta_R$ | $N_{iso}$ | $\Theta_R$ | $N_{iso}$ |
| spinach (I) | 33° | 63° | | 48° | | 76° | |
| | 35° | 65° | 1.9 | 48° | 5.0 | 79° | 0.8 |
| | 37° | 65° | | 48° | | 84° | |
| *S. obliquus* (I) | 36° | 57° | | 57° | | 78° | |
| | 38° | 57° | 1.9 | 58° | 4.9 | 82° | 0.9 |
| | 40° | 57° | | 58° | | (90°)[b] | |
| spinach (II) | 33° | 69° | | 45° | | 78° | |
| | 35° | 70° | 1.9 | 44° | 4.7 | 81° | 1.1 |
| | 37° | 72° | | 43° | | (90°)[b] | |
| *S. obliquus* (II) | 36° | 59° | | 51° | | 76° | |
| | 38° | 59° | 2.1 | 51° | 3.8 | 79° | 1.3 |
| | 40° | 60° | | 50° | | 84° | |

[a] Fits for the experimentally determined mosaic spread angle, $\Omega_{sp}$, $\Omega_{sp}$ + 2°, and $\Omega_{sp}$ − 2° are shown.

## DISCUSSION

*Alga versus Higher Plant.* Manganese K-edge spectra (Figure 2) and EXAFS spectra (Figure 3; Tables 1−6) collected on multilayers of photosystem II-enriched membrane fragments of *S. obliquus*, a unicellular green alga, and spinach, a higher plant, are highly similar. The XAS dichroism data might indicate differences with respect to the height of the third Fourier peak (strength of the 3.3-Å EXAFS interaction) and the orientation of the 1.8-Å vector connecting the absorbing Mn and, presumably, a backscattering $\mu$-O atom. However, despite comparable data aquisition times, XAS data collected for the green alga is significantly more affected by noise than the corresponding data sets collected on spinach preparations. (The number of PS II units per membrane area seems to be lower for green algae membrane preparations than for those of spinach. Consequently, the detected X-ray fluorescence emission was found to be lower by a factor of 2, whereas the scatter background was found to be clearly larger.) Therefore, we attribute the apparent differences to noise contributions. In summary, the PS IIs of the green alga and the higher plant do not differ significantly in the structure of the manganese complex and its orientation with respect to the thylakoid membrane, which hosts the PS II membrane proteins. The reason for the subtle, but fully reproducible, differences in the multiline signal of both organisms (*26*; unpublished results) remains, presently, obscure.

We recently observed a comparable similarity between higher plants and green algae for the $Tyr_D$ radical (Tyr-161 of the D2 protein, a redox-active residue which is not directly involved in water oxidation) by EPR spectroscopy on oriented membrane particles (*27*). Seemingly, the tertiary structure of the protein matrix, which determines the orienta-

tion of the redox factors, is essentially identical at the PS II donor side of green algae and higher plants.

In conclusion, in the course of evolution from unicellular green algae to higher plants, the PS II manganese complex has not been modified. The experimental results obtained for the PS II manganese complex of higher plants are, most probably, equally valid for unicellular green algae (which are better suited for site-directed mutagenesis studies).

*The 2.7-Å Mn−Mn Distance*. We and others (*15*, *36*, *38*, *39*) observe for the PS II manganese complex in its $S_1$-state strong EXAFS interactions which correspond to backscattering atoms at 2.7 Å. Taking into consideration that significant contributions of backscattering oxygen, nitrogen, or carbon atoms to the 2.7-Å EXAFS oscillations are unlikely, this EXAFS interaction is clearly assignable to Mn−Mn distances of 2.7 Å. The coordination number of about 1 backscattering Mn atom per absorbing Mn atom indicates that there are two Mn−Mn distances of 2.7 Å per tetranuclear Mn complex.

Mn−Mn distances close to 2.7 Å are highly suggestive of a structural element containing Mn atoms connected by a di-$\mu$-oxo bridge (*11*, *46*). Therefore, in agreement with most investigators in this field (*3*, *8*, *39*), we assume that the PS II manganese complex contains two $Mn_2(\mu\text{-}O_2)$ structures. It should be noted that the presently available EXAFS data does not exclude that these two $Mn_2(\mu\text{-}O_2)$ elements share a common Mn atom resulting in a trinuclear structure with di-$\mu$-oxo bridges between adjacent Mn atoms (as pointed out, for example, by DeRose et al. (*17*), and as recently also proposed by Semin and Parak (*47*)).

*Resolution of Mn−Ligand Distances of 1.8 and 2.0 Å.* The structural information carried by the first Fourier peak is disputed. Klein and co-workers (*17*, *38*) and others (*39*) frequently used a curve-fitting approach which involves two distinct distances of 1.8 and 2.0 Å, but recently it has been concluded that only a single absorber−backscatterer distance can be resolved (*40*, *48*). We noticed that, indeed, conventional EXAFS spectra on isotropic samples do not allow a firm conclusion with respect to the existence of two distinct backscatterer distances in the first Mn coordination shell. However, for the data collected at 15° on vectorially oriented samples a single-distance approach is certainly insufficient (Figure 7). Furthermore, the pronounced angle dependence of the shape of the EXAFS oscillations corresponding to the first coordination shell (Figure 6A) is an indisputable indication that backscattering atoms at two (or more) distinct distances are involved. Thus, the dichroism approach permits the unequivocal detection of otherwise hidden "subshells" of backscattering atoms.

The finding of two distinct distances contributing to the first shell EXAFS interactions and the corresponding fit results (Tables 2, 3, and 5) suggest that a fraction of the Mn ligands are $\mu$-oxo ligands (typical Mn−$\mu$-O distances are 1.75−1.85 Å, (*11*)), whereas the terminal (meaning non-$\mu$-oxo) ligands are at an average distance of 1.95 Å with a considerable spread of the individual distances (the Debye−Waller factors indicate a distance spread larger than 0.1 Å). In synthetic model compounds distances as short as 1.95 Å are rarely found for nitrogen ligands (e.g., imidazole nitrogen). Thus the 1.95-Å distance provides an indication that the vast majority of terminal Mn ligands are oxygen atoms. However, it should be noted that for a highly heterogeneous backscatterer shell the use of a symmetric Debye−Waller factor for simulation of EXAFS oscillations could result in erroneous values for the average distance. The value for the absorber−backscatterer distance of the terminal ligands is likely to be relatively imprecise.

*The $\Theta_{2.7\text{ Å}}$-Value*. George et al. (*18*), Mukerji et al. (*20*), and Dau et al. (*21*) determined the average angle between the thylakoid membrane normal and the 2.7-Å Mn−Mn vector, $\Theta_{2.7\text{ Å}}$, to be about 60°. Here, we find $\Theta_{2.7\text{ Å}}$ to be close to 80° (Table 6). Information on the orientation of the two $Mn_2(\mu\text{-}O_2)$ blocks should provide reliable constraints for structural models of the PS II manganese complex and for atomic resolution models of the surrounding protein matrix. Therefore, the discrepancy between results presented here and previously published results needs to be resolved. This discrepancy presumably originates from different approaches toward (1) determination of $\Theta_R$ based on $N_{app}(\Theta_E)$, (2) determination of the mosaic spread characteristics, (3) normalization of the EXAFS data, and, perhaps, (4) radiation damage to the manganese complex or its protein environment.

(1) In the present investigation, $\Theta_R$ determination is based on eq 4, whereas previously a relation proposed by George et al. (*18*) had been applied (*15*, *18*, *20*, *21*). George et al. describe the mosaic spread characteristics by using a Gaussian distribution function for the azimuthal angle of the absorber−backscatterer vector ($\Theta_R$ in Figure 8). For the half-width angle of the $\Theta_R$, Gaussian distribution values were used which had been determined for the Gaussian distribution function of membrane normals ($\Omega_{sp}$). This approach is inaccurate, because the $\Theta_R$ distribution function is not identical to the $\Omega_{sp}$ distribution function. By reevaluation of previously published results (*20*, *21*) we found that this inaccurate approach results in values for $\Theta_{2.7\text{ Å}}$ which are 3−5° smaller than values obtained using eq 4. Thus, the discrepancy between the $\Theta_{2.7\text{ Å}}$ value determined in this study and published values (*15*, *18*, *20*, *21*) is partially explainable by this methodical error.

(2) The determination of $\Theta_{2.7\text{ Å}}$ by simulation of the excitation angle dependence requires knowledge of the mosaic spread characteristics of the samples. In previous investigations (*18*, *20*, *21*) the mosaic spread characteristics were determined by comparison of the angle dependence of experimentally determined $Cyt_{b559}$ EPR-signals with numerical simulations using the EPR simulation approach of Blum et al. (*35*). Blum et al. erroneously assume that a given azimuthal angle distribution function for the membrane normal ($P_{ord}(\alpha)$ as defined in the context of Figure 8) translates directly to an identical azimuthal angle distribution function for the orientation of the magnetic field vector with respect to an axis fixed in the paramagnetic molecule. On the basis of this assumption they calculate EPR spectra by taking into consideration all possible orientations of the magnetic field vector with respect to a molecule-fixed coordinate system. A correct approach requires either to consider explicitly all possible orientations of the membrane normal (corresponding to the $\alpha$- and $\beta$-integration path in Figure 8) and of the paramagnetic molecule in the membrane (corresponding to the $\gamma$-integration path in Figure 8) or to calculate the angle distribution function for the magnetic field vector in a molecule-fixed coordinate system as proposed by Friesner et al. (*49*). For the present investigation, we

have chosen the first alternative. In conclusion, in previously published investigations determination of $\Theta_{2.7\,Å}$ involved values for the mosaic spread angle (the half-width angle of the Gaussian distribution function for the membrane normal) which are likely to be incorrect. On the basis of a reevaluation of the $Cyt_{b559}$ EPR data presented in Dau et al. (*21*), we estimate that the incorrect approach of Blum et al. (*35*) had resulted in mosaic spread angles which are about 10° too low.

(3) The X-ray penetration depth increases with increasing excitation energy, *E*, resulting in enhanced X-ray fluorescence for higher excitation energies. For the detection geometry used here and elsewhere (*20*, *21*), at wider excitation angles ($\Theta_E$) the X-ray emission stemming from deeper sample layers is particularly strongly attenuated by fluorescence reabsorption. Consequently, the enhancement of EXAFS oscillation due to the energy-dependent penetration depth affects to a higher extent spectra collected at small $\Theta_E$. In this study, a correction for these intricate penetration-depth effects is achieved by using the actual fluorescence-detected spectrum for normalization of EXAFS oscillations. (It should be noted, however, that this normalization approach is problematic in the case of spectra which are significantly affected by a scattering background.) Previously, an EXAFS normalization method has been used (division by a theoretical post-edge background function in Mukerji et al. (*20*) and Dau et al. (*21*)) which does not fully prevent an artifactual influence of $\Theta_E$ on the EXAFS data.

(4) The use of relatively low X-ray fluxes (about $10^{10}$ photons/mm$^2$/s) and measurement temperatures below 20 K does not prevent the X-ray photoreduction of the manganese complex (see ref *22*); the EXAFS data is affected in the case of irradiation periods exceeding 3 h (see Tables 1, 2, 4, and 5). Even though in this investigation the obtained $\Theta_{2.7\,Å}$ and $\Theta_{1.8\,Å}$ values are essentially identical for short-term irradiation not exceeding 2.5 h (protocol II) and more prolonged irradiation (10−15 h, protocol I), the use of even more prolonged irradiation times or more intense synchrotron radiation could be critical. (We cannot judge whether and to what extent the previously published data of Mukerij et al. (*20*) and Dau et al. (*21*) are affected by photoreduction of the manganese complex because the experimental conditions were different. On one hand, the X-ray fluxes used were larger by, perhaps, 1 order of magnitude; on the other hand, the temperature of the sample during the measurement was lower by a factor of 2.)

*Determination of* $\Theta_{1.8\,Å}$. The first shell EXAFS data is often severely affected by the background removal procedure. Here, mainly due to improved samples, the X-ray spectra were essentially free of any background which results from scattered X-rays (zero slope of the pre-edge background, unusually flat background in the EXAFS range). Consequently, the background removal procedure was not as critical as it had been in previous investigations. The lowered distortion by background artifacts enabled detection and quantitative evaluation of the dichroism in the first shell EXAFS data.

Because the information content of the first EXAFS Fourier peak is limited, the use of a model-dependent fit approach to determine the angle dependence of the apparent coordination numbers of the 1.8- and 1.95-Å distances is advisable (see Results). Here, on the basis of the 2.7-Å EXAFS data, the supposition is used that there are two $\mu$-oxo ligands at ∼1.8 Å and four ligands at longer distances per absorbing Mn atom. However, the 2.7-Å EXAFS data do not provide any evidence against more than four $\mu$-oxo bridges per tetranuclear manganese complex (e.g., the model of Yachandra et al. (*15*) predicts 2.5 $\mu$-oxo ligands per manganese). Furthermore, the fit approach involves the assumption that the distance values for the shorter and the longer distance, which constitute average distances, are fully angle independent, which may or may not be a good approximation.

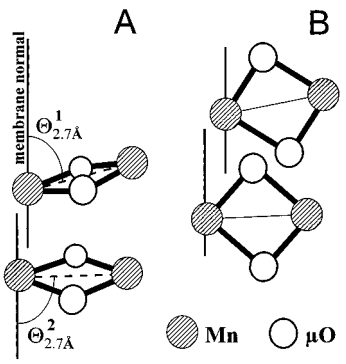


FIGURE 10: Orientation of the two di-$\mu$-oxo-bridged binuclear manganese units. The average angle of $\Theta^1_{2.7\,Å}$ and $\Theta^2_{2.7\,Å}$ is close to 80° as indicated by the dichroism of the 2.7-Å EXAFS. Panels A and B differ with respect to the orientation of the $Mn_2(\mu\text{-}O_2)$ plane. The orientation of the $Mn_2(\mu\text{-}O_2)$ plane shown in panel B is not in agreement with the dichroism of the 1.8-Å EXAFS.

In conclusion, the preferential orientation of the Mn−$\mu$-O vector is perpendicular rather than parallel to the membrane normal. However, due to possible insufficiencies of the fit approach, the obtained $\Theta_{1.8\,Å}$ and $\Theta_{2.0\,Å}$ values are likely to be relatively imprecise.

*Orientation of* $Mn_2(\mu\text{-}O_2)$ *Structures.* According to the presented EXAFS dichroism results, in the manganese complex two $Mn_2(\mu\text{-}O)_2$ blocks are arranged such that two Mn−Mn vectors are at an average angle of ∼80° with respect to the thylakoid membrane normal. This result imposes restrictions on the orientation of the individual Mn−Mn vectors. By eq 6 we determine that for $\Theta^1_{2.7\,Å}$ equal to 90°, $\Theta^2_{2.7\,Å}$ equals 76°. Thus, for an average angle of 80° the individual angles differ by maximally 14°.

In Figure 10 two alternative arrangements of the $Mn_2(\mu\text{-}O_2)$ blocks are shown which are equivalent with respect to the orientation of the 2.7-Å Mn−Mn vectors, but which differ with respect to the orientation of the $Mn_2(\mu\text{-}O_2)$ plane. The arrangement shown in Figure 10B is not in agreement with the dichroism of the 1.8-Å vector.

As discussed above, the results of this investigation impose restrictions on possible models for structure and orientation of the PS II manganese complex. The Berkeley model (*8*, *15*; see Introduction), with respect to the proposed structure, is in good agreement and, with respect to the originally proposed orientation (*15*, *20*, *21*), in qualitative agreement with the results of this XAS linear dichroism investigation. It remains to be elucidated whether alternative models are equally well in agreement with the results presented here.

## ACKNOWLEDGMENT

We thank Drs. O. Burghaus and C. Elschenbroich (Marburg) for technical support with respect to the EPR measure-

ments. We are grateful to Drs. H. Senger, D. Dörnemann, R. Schulz, and A. Batschauer (Marburg) for supporting this investigation in various ways. We thank the staff of the mechanics workshop of the FB Biologie for the skillful making of XAS sample holders and centrifuge tubes. S. Klingelhöfer and I. Heinze (Marburg) had been involved in initial work on the manganese complex of *S. obliquus*. H.D. thanks Drs. K. Sauer, M. Klein, V. Yachandra (Berkeley), and their co-workers for the joint investigations in 1992, which stimulated this work.

## REFERENCES

1. Rutherford, A. W., Zimmermann, J.-L., and Boussac, A. (1992) in *The Photosystems: Structure, Function and Molecular Biology* (Barber, J., Ed.) pp 179−229, Elsevier, Amsterdam, The Netherlands.
2. Debus, R. J. (1992) *Biochim. Biophys. Acta 1102*, 269−352.
3. Riggs-Gelasco, P. J., Mei, R., and Penner-Hahn, J. E. (1995) *Adv. Chem. Ser. 246*, 219−248.
4. Haumann, M., and Junge, W. (1996) in *Oxygenic Photosynthesis: The Light Reactions* (Ort, D. R., and Yocum, C. F., Eds.) pp 165−192, Kluwer Academic Publishers, Dordrecht, The Netherlands.
5. Britt, R. D. (1996) in *Oxygenic Photosynthesis: The Light Reactions* (Ort, D. R., and Yocum, C. F., Eds.) pp 137−164, Kluwer Academic Publishers, Dordrecht, The Netherlands.
6. Yachandra, V. K., Sauer K., and Klein, M. P. (1996) *Chem. Rev. 96*, 2927−2950.
7. Vermaas, W. (1993) *Annu. Rev. Plant Physiol. Plant Mol. Biol. 44*, 457−481.
8. Sauer, K., Yachandra, V. K., Britt, R. D., and Klein, M. P. (1992) in *Manganese Redox Enzymes* (Pecoraro, V. L., Ed.) pp 141−175, VCH, Weinheim, Germany.
9. Rüttinger, W., and Dismukes, G. C. (1997) *Chem. Rev. 97*, 1−24.
10. Brudvig, G. W., and Crabtree, R. H. (1986) *Proc. Natl. Acad. Sci. U.S.A. 83*, 4586−4588.
11. Wieghardt, K. (1989) *Angew. Chem., Int. Ed. Engl. 28*, 1153−1172.
12. Pecoraro, V. L. (1992) in *Manganese Redox Enzymes* (Pecoraro, V. L., Ed.) pp 197−231, VCH, Weinheim, Germany.
13. Renger, G. (1993) *Photosynth. Res. 38*, 229−247.
14. Hoganson, C. W., and Babcock, G. T. (1997) *Science 277*, 1953−1956.
15. Yachandra, V. K., DeRose, V. J., Latimer, M. J., Mukerji, I., Sauer, K., and Klein, M. P. (1993) *Science 260*, 675−679.
16. Shriver, D. F., Atkins, P. W., and Langford, C. H. (1994) in *Inorganic Chemistry*, Oxford University Press, Oxford, U.K.
17. DeRose, V. J., Mukerji, I., Latimer, M. J., Yachandra, V. K., Sauer, K., and Klein, M. P. (1994) *J. Am. Chem. Soc. 116*, 5239−5249.
18. George, G. N., Prince, R. C., and Cramer, S. P. (1989) *Science 243*, 789−791.
19. George, G. N., Cramer, S. P., Frey, T. G., and Prince, R. C. (1993) *Biochim. Biophys. Acta 1142*, 240−252.
20. Mukerji, I., Andrews, J. C., DeRose, V. J., Latimer, M. J., Yachandra, V. K., Sauer, K., and Klein, M. P. (1994) *Biochemistry 33*, 9712−9721.
21. Dau, H., Andrews, J. C., Roelofs, T. A., Latimer, M. J., Liang, W., Yachandra, V. K., Sauer, K., and Klein, M. P. (1995) *Biochemistry 34*, 5274−5287.
22. Dau, H., Dittmer, J., Iuzzolino, L., Schiller, H., Dörner, W., Heinze, I., Sole, V. A., and Nolting, H.-F. (1997) *J. Phys. IV 7*, 607−610.
23. McDermott, A. E., Yachandra, V. K., Guiles, R. D., Cole, J. L., Dexheimer, S. L., Britt, R. D., Sauer, K., and Klein, M. P. (1988) *Biochemistry 27*, 4021−4031.
24. Barry, B. A., Boerner, R. J., and de Paula, J. C. (1994) in *The Molecular Biology of Cyanobacteria* (Bryant, D. A., Ed.) pp 217−257, Kluwer Academic Publishers, Dordrecht, The Netherlands.
25. Rigby, S. E. J., Nugent, J. H. A., and O'Malley, P. J. (1994) *Biochemistry 33*, 1734−1742.
26. Schiller, H., Klingelhöfer, S., Dörner, W., Senger, H., and Dau, H. (1995) in *Photosynthesis: from Light to Biosphere* (Mathis P., Ed.) Vol. II, pp 463−466, Kluwer Academic Publishers, Dordrecht, The Netherlands.
27. Schiller, H., Iuzzolino, L., Dittmer, J., and Dau, H. (1996) *Ber. Bunsen-Ges. Phys. Chem. 100*, 1999−2002.
28. Johanningmeier, U., and Heiss, S. (1993) *Plant Mol. Biol. 22*, 91−99.
29. Minagawa, J., and Crofts, A. R. (1994) *Photosynth. Res. 42*, 121−131.
30. Senger, H., and Mell, V. (1977) *Methods Cell Biol. 15*, 201−219.
31. Rutherford, A. W. (1985) *Biochim. Biophys. Acta 807*, 189−201.
32. Dismukes, G. C., and Siderer, Y. (1981) *Proc. Natl. Acad. Sci. U.S.A.* 78, 274−278.
33. Pettifer, R. F., and Hermes C. (1985) *J. Appl. Crystallogr. 18*, 404−412.
34. Gurman, S. J., Binsted, N., and Ross, I. (1984) *J. Phys. C: Solid State Phys. 17*, 143−151.
35. Blum, H., Salerno, J. C., and Leigh, J. S., Jr., (1978) *J. Magn. Reson. 30*, 385−391.
36. Penner-Hahn, J. E., Fronko, R. M., Pecoraro, V. L., Yocum, C. F., Betts, S. D., and Bowlby, N. R. (1990) *J. Am. Chem. Soc. 112*, 2549−2557.
37. Bossek, U., Hummel, H., Weyhermüller, T., Wieghardt, K., Russel, S., v. der Wolf, L., and Kolb, U. (1996) *Angew. Chem., Int. Ed. Engl. 35*, 1552−1554.
38. Yachandra, V. K., Guiles, R. D., McDermott, A., Britt, R. D., Dexheimer, S. L., Sauer, K., and Klein, M. P. (1986) *Biochim. Biophys. Acta 850*, 324−332.
39. MacLachlan, D. J., Hallahan, B. J., Ruffle, S. V., Nugent, J. H. A., Evans, M. C. W., Strange, R. W., and Hasnain, S. S. (1992) *Biochem. J. 285*, 569−576.
40. Latimer, M. J., DeRose, V. J., Mukerji, I., Yachandra, V. K., Sauer, K., and Klein, M. P. (1995) *Biochemistry 34*, 10898−10909.
41. Riggs-Gelasco, P. J., Mei, R., Ghanotakis, D. F., Yocum, C. F., and Penner-Hahn, J. E. (1996) *J. Am. Chem. Soc. 118*, 2400−2410.
42. MacLachlan, D. J., Nugent, J. H. A., Bratt, P. J., and Evans, M. C. W. (1994) *Biochim. Biophys. Acta 1186*, 186−200.
43. Dittmer, J., and Dau, H. (1996) *Ber. Bunsen-Ges. Phys. Chem. 100*, 1993−1998.
44. Pecoraro, V. L., Baldwin, M. J., and Gelasco, A. (1994) *Chem. Rev. 94*, 807−826.
45. Larson, E. J., and Pecoraro, V. L. (1992) in *Manganese Redox Enzymes* (Pecoraro, V. L., Ed.) pp 1−28, VCH, Weinheim, Germany.
46. Gurman, S. J. (1988) *J. Phys. C: Solid State Phys. 21*, 3699−3717.
47. Semin, B. K., and Parak, F. (1997) *FEBS Lett. 400*, 259−262.
48. Riggs-Gelasco, P. J., Mei, R., Yocum, C. F., and Penner-Hahn, J. E. (1996) *J. Am. Chem. Soc. 118*, 2387−2399.
49. Friesner, R., Nairn, J. A., and Sauer, K. (1980) *J. Chem. Phys. 72*, 221−230.

BI972329B